Comparison of bulk-sensitive spectroscopic probes of Yb valence in Kondo systems

L. Moreschini,[1] C. Dallera,[2] J. J. Joyce,[3] J. L. Sarrao,[3] E. D. Bauer,[3] V. Fritsch,[3] S. Bobev,[3] E. Carpene,[2] S. Huotari,[4] G. Vankó,[4] G. Monaco,[4] P. Lacovig,[5] G. Panaccione,[5] A. Fondacaro,[6] G. Paolicelli,[6] P. Torelli,[7] and M. Grioni[1]

[1]*IPN, Ecole Polytechnique Fédérale (EPFL), CH-1015 Lausanne, Switzerland*
[2]*INFM-Dipartimento di Fisica, Politecnico di Milano, p. Leonardo da Vinci 32, 20133 Milano, Italy*
[3]*Los Alamos National Laboratory, Los Alamos, New Mexico 87545, USA*
[4]*European Synchrotron Radiation Facility (ESRF), 38043 Grenoble Cedex, France*
[5]*Laboratorio TASC, INFM, Area Science Park, S.S. 14, Km 163.5, Basovizza, Italy*
[6]*INFM and Dipartimento di Fisica, Universitá di Roma III, I-00146 Roma, Italy*
[7]*LURE, Université de Paris–Sud, F-91898 Orsay, France*

(Received 16 August 2006; revised manuscript received 17 October 2006; published 11 January 2007)

We exploited complementary synchrotron radiation spectroscopies to study the Yb 4*f* electronic configuration in three representative intermediate-valence materials: $YbAl_3$, $YbInCu_4$, and $YbCu_2Si_2$. High-resolution x-ray absorption (PFY-XAS), resonant inelastic x-ray scattering (RIXS), and hard-x-ray photoemission (HAXPES) data all show characteristic temperature-dependent changes of the Yb valence. For each material, the increments measured from low (20 K) to high (300 K) temperature by the different probes are quite similar. The estimated RIXS and XAS valences are consistently higher than the HAXPES values. We briefly discuss the possible origin of this discrepancy.

DOI: 10.1103/PhysRevB.75.035113 PACS number(s): 71.28.+d, 78.70.En, 78.70.Dm, 79.60.−i

I. INTRODUCTION

High-energy spectroscopies such as photoemission (PES) or x-ray absorption (XAS) provide unique insight into the dynamics of the 4*f* electrons in intermediate valence compounds (IVC), like many Ce or Yb intermetallics.[1–3] The fractional occupancy n_f of these states reflects their hybridization with extended conduction-band electrons, which is at the origin of the "Kondo" phenomena in these materials. The Anderson impurity model (AIM), which embodies the minimal theoretical description of this phenomenon, predicts for n_f a simple dependence on hybridization and temperature,[4] via the single parameter (T/T_K). T_K is the material-dependent Kondo temperature, which grows exponentially with the 4*f*-band hybridization, and sets the low-energy scale of the problem. It is generally assumed that these generic features of the AIM survive in the more elaborate and applicable theoretical lattice schemes.[5]

Some aspects of the predicted T/T_K dependence have been confirmed qualitatively by conventional XAS (Refs. 6–8) and core-level PES,[9] and even quantitatively by more elaborate photon-in–photon-out experiments.[10] Such spectroscopic "Kondo scaling" should be especially evident in valence-band PES data, since the intensity of the Kondo resonance (KR), the characteristic many-body feature straddling the Fermi level,[4,11] directly reflects the configuration mixing in the ground state. PES data, on the contrary, have been controversial, with results from cleaved single crystals[12,13] failing to exhibit the T/T_K dependence generally observed in polycrystalline samples.[2,3,14–16] The issue is confused by the short probing depth (5–10 Å) of low-energy PES, and by the tendency of the Yb (Ce) ions to adopt a surface electronic configuration different from that of the bulk. Soft-[17–21] and hard-x-ray PES (HAXPES) (Refs. 20 and 22) experiments with enhanced bulk sensitivity generally support a Kondo scenario interpretation.

The purpose of the present paper is to compare HAXPES with two novel and intrinsically bulk-sensitive photon-in–photon-out spectroscopies: "high-resolution" XAS and resonant inelastic x-ray spectroscopy (RIXS).[23] This issue has already been addressed in the literature, e.g., in Ref. 21. Here, we set out to collect a broad and consistent data set, using a state-of-the-art synchrotron apparatus combining both capabilities. We present results on three representative Yb IVC's: $YbAl_3$, $YbInCu_4$, and $YbCu_2Si_2$. All these systems have been extensively studied by PES and XAS, and therefore represent an excellent benchmark for our comparison of spectroscopic probes. $YbCu_2Si_2$ and $YbAl_3$ are typical Kondo systems, with Kondo temperatures $T_K \sim 40-60$ K and, respectively, $T_K \sim 400$ K.[12,14] $YbInCu_4$ exhibits at $T_V = 42$ K an isostructural first-order transition that affects the electronic and magnetic properties. The valence suddenly increases from 2.83 to 2.96 for $T > T_V$, while the Kondo temperature drops from $T_K \sim 400$ K $(T < T_V)$ to $T_K \sim 20$ K $(T > T_V)$.[24,25]

We show that the different spectroscopies agree on two major points. First, they all indicate an increase of the Yb valence (at 20 K) from $YbAl_3$ to $YbCu_2Si_2$, in agreement with the known properties of the three compounds. Secondly, they reveal the expected increase of the Yb valence with temperature. The valence values extracted from the XAS/RIXS data are closer to the estimates from nonspectroscopic measurements. HAXPES provides a more direct view of the Yb 4*f* states, but remains more sensitive to the sample preparation procedure. In our experiment, the perturbation produced by scraping the surface may well have extended over a thickness comparable to—and possibly larger than—the probing depth of HAXPES (~60 Å). We conclude that XAS/RIXS is the more consistent probe of the bulk Yb electronic configuration.

 ©2007 The American Physical Society

II. EXPERIMENTAL

We have used flux-grown single crystals characterized by x-ray diffraction and magnetic susceptibility measurements. All measurements were performed at the undulator beamline ID16 of the ESRF (Grenoble) equipped with a Si(111) double-crystal monochromator. Both photon-in–photon-out (XAS, RIXS) and HAXPES experiments can be performed at this beamline. For XAS and RIXS experiments, freshly scraped samples were mounted on a He cryostat and measured in high (10^{-8} mbar) vacuum. We used a Rowland circle spectrometer based on a spherically bent Si(620) crystal, and a Si avalanche photodiode detector. The total energy resolution was $\sim$1.5 eV. For HAXPES, the beamline was equipped with a Si(333) channel-cut post-monochromator working in near backscattering condition at $h\nu$=5935 eV. The samples were scraped by a diamond file at 10^{-9} mbar, and measured by the VOLPE electron spectrometer.[26] The combined (photons+electrons) energy resolution now attainable by this instrument is $\Delta E \sim 70$ meV, but for the present experiment we used a lower-resolution $\Delta E \sim 0.25$ eV in a trade-off for intensity.

III. RESULTS AND DISCUSSION

"High-resolution" partial fluorescence yield x-ray absorption (PFY-XAS) is an evolution of XAS that exploits the enhanced flux and brilliance of modern synchrotrons. In a conventional "total yield" XAS experiment, the secondary electrons (electron yield) or photons (fluorescence yield) emitted after the absorption of x rays are collected with no further energy analysis. Their intensity, measured as a function of the incident photon energy, is proportional to the absorption coefficient. XAS, namely in the fluorescence mode, is truly bulk-sensitive, with a probing depth in the μm range for core-level binding energies of several keV's. Its main drawback is the large spectral broadening associated with the short lifetime of the deep core hole in its final state. For the Yb $2p_{3/2}$ (L_3) edge, the lifetime broadening is $\Delta E \sim 5.3$ eV.[27]

In PFY-XAS experiments, only the intensity of a specific fluorescence channel is measured. They are technically more complex, in that they require an energy analysis of the secondary photon beam. In our Yb L_3 PFY-XAS experiment, we measured, as a function of the incident photon energy $h\nu_{\rm in}$, the intensity of the $L\alpha_1$ ($3d \rightarrow 2p$) fluorescence ($h\nu_0$ =7415 eV) emitted after the creation of a Yb $2p$ hole: $2p^6 4f^N \rightarrow 2p^5 4f^N \varepsilon d \rightarrow 2p^6 3d^9 4f^N$. The probing depth of Yb L_3 PFY-XAS is similar to that of standard XAS, but the selection of a specific final state brings an important advantage. In fact, the intrinsic spectral linewidth is set by the shallower $3d$ hole ($\Delta E \sim 0.6$ eV), rather than by the deep $2p$ hole. Even if a careful theoretical analysis shows that the PFY-XAS spectrum is not strictly identical to XAS with a reduced linewidth, PFY-XAS is of great value, because it gives access to finer spectral details.[23,28,29] Unlike PFY-XAS, RIXS experiments record, for each value of $h\nu_{\rm in}$, the whole energy distribution of the photons emitted after the x-ray absorption. RIXS is therefore closely related to PFY-XAS, but potentially much richer in information if the whole ($h\nu_{\rm in}, h\nu_{\rm out}$) parameter space is explored.[23] The energy transfer $E_T = (h\nu_{\rm in} - h\nu_{\rm out})$ is the energy transferred from the scattered photon to the solid, i.e., the energy difference between the excited final state and the ground state. In the following, RIXS data are plotted as the function of the relative energy transfer E_T-E_0, where E_0=1526 eV is the Yb $3d_{5/2}$ threshold.

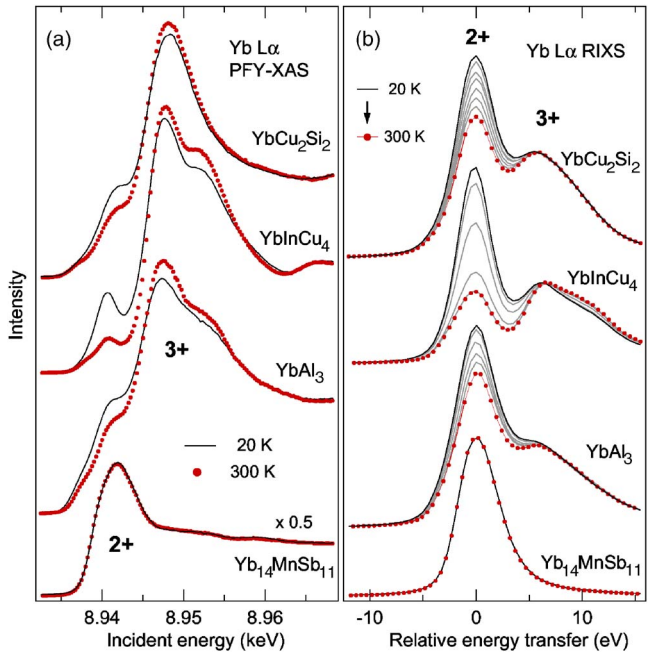

FIG. 1. (Color online) (a) PFY-XAS spectra of three IV compounds and of divalent $Yb_{14}MnSb_{11}$ at 20 and 300 K. (b) RIXS spectra measured between 20 and 300 K, at $h\nu_{\rm in}$=8.941 keV, the maximum of the Yb^{2+} resonance profile.

The PFY-XAS and RIXS results for the three IVC's and for the divalent reference compound $Yb_{14}MnSb_{11}$ are summarized in Fig. 1. In Yb IVC's, the L_3 (PFY-)XAS spectrum is a superposition of absorption spectra from the Yb^{2+} and Yb^{3+} components of the hybrid ground state. In our analysis, the intensity of each contribution is assumed to be proportional to the weight of the corresponding initial-state configuration.[8] The spectra of Fig. 1(a) exhibit prominent Yb^{3+} features at 8948 eV and smaller Yb^{2+} signals at $\sim$7 eV lower energy. Spectral weight is transferred from the 2+ to the 3+ component at the higher temperature in all the IVC systems, following the increase of the Yb valence predicted by a Kondo scenario.[4,10]

The RIXS spectra similarly exhibit Yb^{2+} and Yb^{3+} components, which can be selectively enhanced by an appropriate choice of the incident photon energy. The spectra of Fig. 1(b) correspond to the incident energy ($h\nu$=8941 eV) where the Yb^{2+} XAS and RIXS signals are largest. This is a favorable condition because small valence changes have a larger effect on the minority Yb^{2+} weight, which is proportional to (1-n_h), where n_h is the number of $4f$ holes. For instance, for a Δv=0.1 valence change between v=2.9 (n_h=0.9) and v =2.8 (n_h=0.8), which are typical values for Yb Kondo systems, the Yb^{2+} intensity doubles, but the Yb^{3+} signal only changes by 11%.

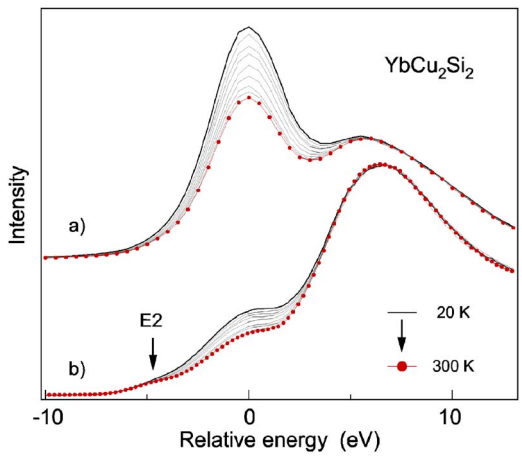

FIG. 2. (Color online) (a) Temperature-dependent RIXS spectra of $YbCu_2Si_2$ from Fig. 1, and (b) the corresponding PFY-XAS spectra. The arrow marks the quadrupole (E2) $2p \rightarrow 4f$ transition. In both cases, all spectra were normalized to the maximum of the Yb^{3+} signal.

The practical—if not fundamental—advantage offered by RIXS in this context is well illustrated by Fig. 2, which compares the full PFY-XAS and RIXS temperature dependence for $YbCu_2Si_2$. In both cases, the spectra were normalized for convenience to the maximum of their respective Yb^{3+} signal. The weak preedge feature at ~ -4 eV in PFY-XAS reflects a quadrupole-allowed ($E2$) $2p^6 4f^{13} \rightarrow 2p^5 4f^{14}$ transition from the Yb^{3+} part of the ground state. The temperature-dependent changes in the two sets of data are qualitatively similar, but are clearly more visible in the RIXS spectra due to the selective amplification of the Yb^{2+} signal. Moreover, as shown by a direct comparison of Figs. 1(a) and 1(b), the RIXS line shape is simpler. It lacks the steplike background components—one for each valence state—that need to be phenomenologically introduced in the treatment of the XAS spectra.[8] With fewer free parameters, the quantitative analysis of the RIXS curves is more straightforward. Figure 3 illustrates a typical line-shape analysis, for the 20 K RIXS spectrum of $YbCu_2Si_2$, performed with distinct Yb^{2+} and Yb^{3+} spectral components. The former is a replica of the

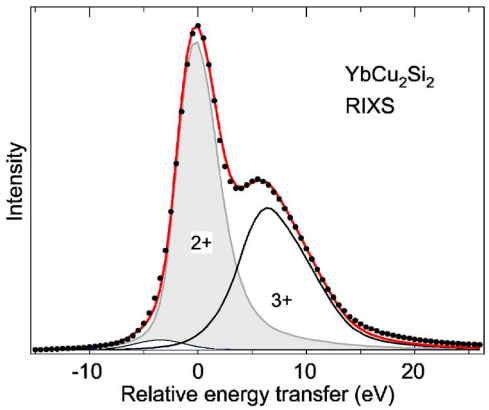

FIG. 3. (Color online) A fit (solid line, color) of the 20 K RIXS spectrum of $YbCu_2Si_2$ obtained as the sum of Yb^{2+}, Yb^{3+}, and E2 components, as described in the text.

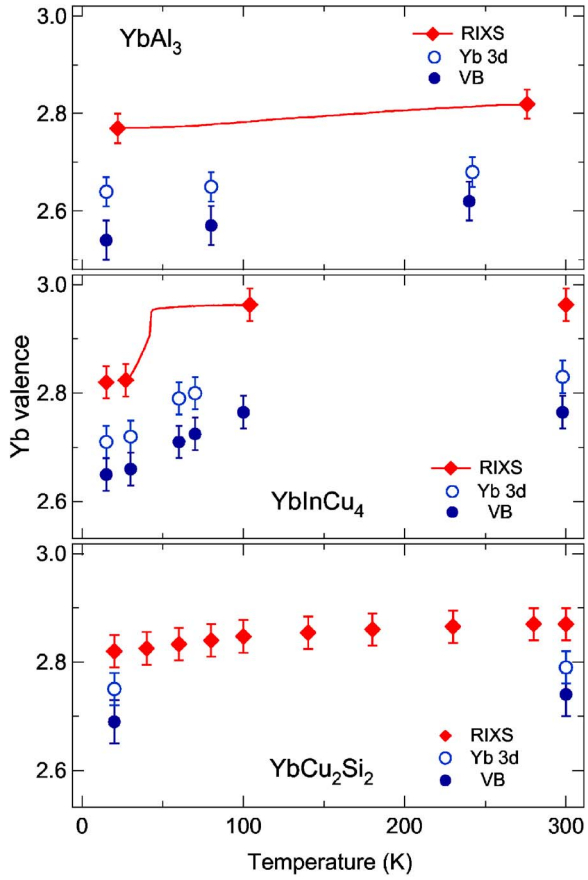

FIG. 4. (Color online) Summary of the valence values determined by the various spectroscopies. The solid lines refer to continuous temperature-dependent RIXS measurements.

RIXS spectrum of the divalent reference compound $Yb_{14}MnSb_{11}$ of Fig. 1. The latter is the RIXS spectrum of $YbCu_2Si_2$, measured at the maximum of the 3+ resonance, i.e., for an incident energy 7 eV above the 2+ resonance. The fit, performed leaving the intensities and energy separation of the Yb^{2+} and Yb^{3+} components unconstrained, has a very small residue around -4 eV, in correspondence with the expected $E2$ transition. A refined three-component fit (solid line, in color) reproduces very well the experimental data.

Changes in the Yb^{2+} RIXS intensity reflect corresponding *relative* changes of the Yb^{2+} weight in the initial state. Knowledge of the Yb valence at one temperature, e.g., at 300 K, is required for a complete determination of the valence $v(T)$. This information can be extracted from the XAS spectrum, as in Ref. 8. It can also be obtained using only RIXS data, by comparing the intensities of the Yb^{2+} and Yb^{3+} signals at the maxima of their respective resonance profiles, as discussed in Ref. 29. The corresponding values are reported in Fig. 4. For $YbAl_3$ and $YbInCu_4$, we also performed continuous measurements of the Yb^{2+} RIXS intensity while changing the temperature at a rate of ~ 1 K/min. $v(T)$ follows a smooth "Kondo" dependence in $YbAl_3$, and the overall valence increase is $\Delta v = 0.05$. In $YbInCu_4$, the Yb valence exhibits a jump at $T_V = 42$ K, and no further evolution above T_V, as expected from $T_K \sim 20$ K in the high-temperature phase. $v(T)$ does not saturate to the

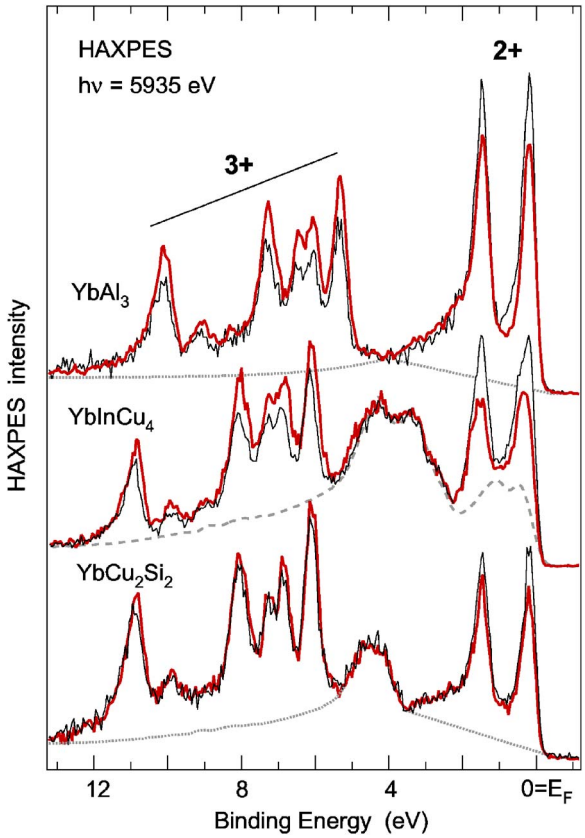

FIG. 5. (Color online) HAXPES ($h\nu$=5935 eV) valence-band spectra measured at 20 K (thin solid lines) and 300 K [thick (red) solid lines]. The dashed line is the spectrum of $LuInCu_4$, after subtraction of the atomiclike Lu 4f doublet. The dotted lines are phenomenological non-4f backgrounds (see text).

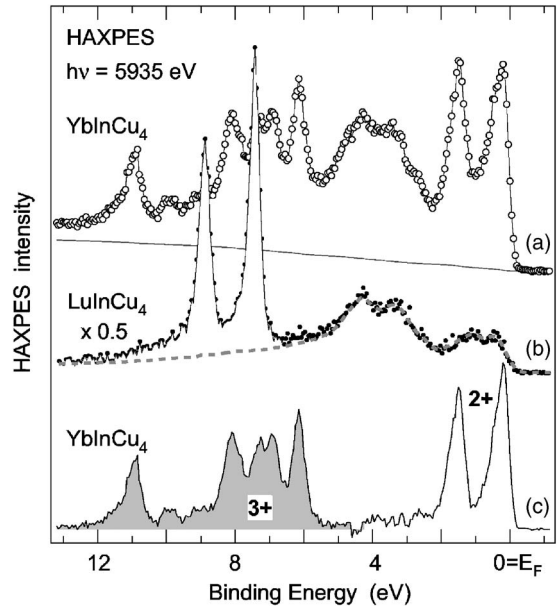

FIG. 6. (a) VB HAXPES spectrum of $YbInCu_4$ (20 K, raw data, empty symbols), and the calculated inelastic background (solid line). (b) VB HAXPES spectrum of $LuInCu_4$ (solid symbols, after removal of the inelastic background). The dashed line, obtained by removing the sharp Lu 4f doublet, represents the contribution from non-4f states. The non-4f and inelastic backgrounds are subtracted from the $YbInCu_4$ spectrum, to obtain the experimental 4f signal shown in (c).

low-T value immediately below T_V, in contrast to the electrical resistivity or the magnetic susceptibility.[25] The further low-T evolution suggests a distribution of T_V's, possibly associated with disorder induced by scraping, and extending over a distance comparable with the probing depth of RIXS. This is much larger than the thickness of a proposed perturbed region under a cleaved surface, as estimated by PES.[21] We speculate that the large mechanical energy dissipated during the scraping process may induce a large density of structural defects throughout a thick subsurface region. Whereas this is almost certainly a general result of scraping, the effect is especially noticeable in the case of $YbInCu_4$ because of the influence of defects on the first-order electronic phase transition. Nonetheless, the RIXS data of Fig. 4 are clear spectroscopic evidence of a first-order-like transition at T_V.

The valence-band (VB) HAXPES results are shown in Fig. 5, after the usual subtraction of inelastic Shirley backgrounds. They exhibit the typical features of Yb IVC's: the spin-orbit-split Yb^{2+} KR near E_F and a Yb^{3+} multiplet at 5–12 eV. Peaks at ~4 eV in $YbInCu_4$ and $YbCu_2Si_2$ are from Cu 3d states. At this photon energy ($h\nu$=5935 eV), the contribution from the topmost surface layer is small (~5%),[30] and the spectra are free from the broad surface signal typical of low-energy PES. The Yb^{3+} intensity in $YbInCu_4$ is somewhat smaller than in published HAXPES data from a fractured sample.[22] The (Yb^{2+}/Yb^{3+}) intensity ratio at 300 K is largest for $YbAl_3$ and smallest for $YbInCu_4$. In all compounds, the intensity of the divalent doublet decreases at high temperature, with a corresponding growth of the Yb^{3+} multiplet. Notice that the simple thermal broadening of the Fermi edge would not affect the integrated intensity of a band feature. The VB HAXPES results are therefore qualitatively consistent with the RIXS data of Fig. 1, and with a Kondo scenario.

The Yb valence can be estimated from the Yb^{2+} and Yb^{3+} VB PES intensities as $v=2+14I^{(3+)}/(14I^{(3+)}+13I^{(2+)})$, after separating the 4$f$ spectrum from overlapping non-4f contributions. This operation can be performed in the most reliable way when isostructural La or Lu substitutes of the Yb compound are available and can be measured in the same conditions. In our experiment, we could measure HAXPES data of $LuInCu_4$, a sister compound of $YbInCu_4$. The VB spectrum of $LuInCu_4$, shown in Fig. 6(b), exhibits a clearly identified nearly-atomic-like Lu 4f doublet at around ~8 eV, which can easily be removed to obtain the dashed line in Fig. 6(b). This spectrum, also reproduced in Fig. 5, represents the non-4f background to the $YbInCu_4$ valence band. Subtraction of this background (and of the inelastic Shirley background) from the 20 K data yields the 4f spectrum of Fig. 6(c). After an integration over separate 2+ and 3+ energy windows, one obtains $v(20\text{ K})=(2.65\pm0.03)$. A similar analysis yields $v(300\text{ K})=(2.77\pm0.03)$. By comparison, subtracting only a sloping background from the 3+ region of the raw spectra of Fig. 5, a procedure that certainly overestimates the Yb^{2+} signal, one would obtain $v_0(20\text{ K})=2.50$.

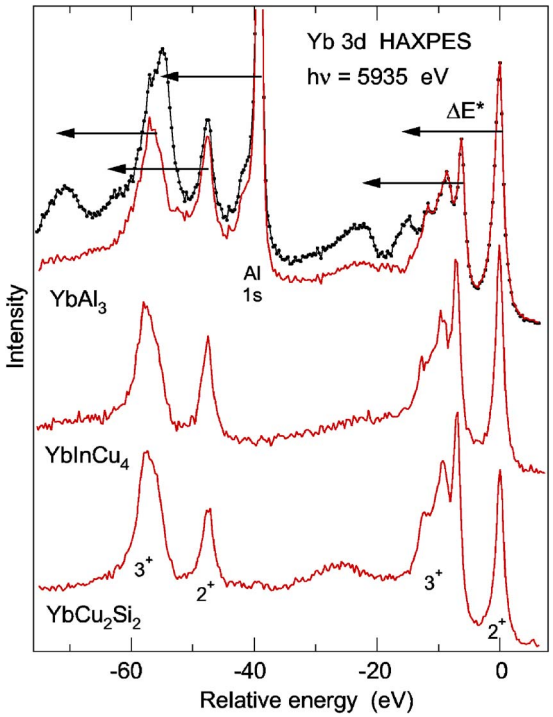

FIG. 7. (Color online) Low-temperature spectra of the Yb $3d$ core levels. Each spin-orbit manifold is split into 2+ and 3+ components. For the $YbAl_3$ spectrum, horizontal arrows identify strong plasmon satellites, shifted by $\Delta E^* \sim 15.2$ eV from the main spectral features. The difference spectrum shown as a solid line is obtained subtracting from the raw spectrum (dots) a scaled replica of the same line shape, shifted by ΔE^*.

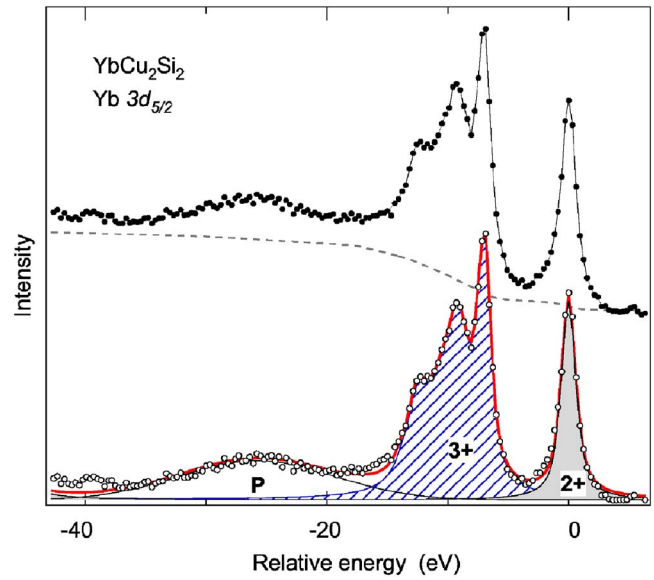

FIG. 8. (Color online) The Yb $3d_{5/2}$ difference spectrum of $YbCu_2Si_2$ obtained by subtraction of a Shirley background (dashed line) from the raw data (solid symbols) is further decomposed into Yb^{2+} and Yb^{3+} components, plus a broad plasmon peak (P), as described in the text.

For $YbAl_3$ and $YbCu_2Si_2$, the corresponding Lu compounds could not be measured. Subtracting the 3+ sloping background and integrating over the Yb^{2+} and Yb^{3+} energy windows yields $v_0(20\text{ K})=2.47$ for $YbAl_3$ and $v_0(20\text{ K})=2.63$ for $YbCu_2Si_2$. To refine these estimates, we used information from published soft-x-ray VB spectra.[12] At $\sim$100 eV, the intensity ratio between the divalent $4f$ and the underlying non-$4f$ emission is $\sim$6 for $YbInCu_4$ and $\sim$15 for both $YbAl_3$ and $YbCu_2Si_2$. Assuming, as a first approximation, similar photon energy dependences for the $4f$/(non-$4f$) intensity ratio as in $YbInCu_4$, and knowing that the non-$4f$ background leads to a $\Delta v=0.15$ correction for $YbInCu_4$, we get from simple algebra $\Delta v \sim 0.06$ for both $YbAl_3$ and $YbCu_2Si_2$. The corrected values are reported in Fig. 4. Subtracting phenomenological backgrounds from the spectra (dotted lines in Fig. 5) would yield compatible results within the error bars. The estimated relative uncertainty of our analysis on the number of $4f$ holes $\Delta n_h/(1-n_h)$ is at the 10% level, which we consider acceptable, since our goal is to compare the different probes, rather than to determine the Yb valence with high accuracy.

The $3d$ core levels are traditional spectroscopic indicators of the electronic configuration in $4f$ materials. Their atomiclike $3d$ lines are well suited to a quantitative analysis, often better than shallower—e.g., $4d$—core levels, which suffer from broader overlapping line shapes. In Yb, the $3d$ levels are too deep for standard Al $K\alpha$ sources, but can easily be reached by HAXPES. In the $3d$ spectra of Fig. 7, the $j=3/2$ and $5/2$ spin-orbit-split manifolds are separated by $\sim$50 eV, and further split into a sharp peak corresponding to the $3d^9 4f^{14}$ (Yb^{2+}) final state and a $3d^9 4f^{13}$ (Yb^{3+}) multiplet. Broad plasmon features are observed at ~ -25 eV, with different intensity in the three compounds, as already noticed in Ref. 22. The case of $YbAl_3$ (dotted line) is peculiar in that several structures are clearly visible besides the Yb $3d$ features. The very intense and strong peak at -40 eV is the Al $1s$ line. All other extra features represent plasmon replicas, which are especially strong in this material. They are all shifted by the same energy $\Delta E \sim 15.2$ eV from the main spectral lines, as indicated by horizontal arrows in the figure. The extrinsic nature of these features is demonstrated by subtracting from the raw data a shifted and reduced replica of the same line shape. The resulting difference spectrum, also shown in Fig. 7 (solid line), is in fact essentially free from the plasmon satellites.

For all three compounds, we have determined the Yb valence by integrating the intensity of the $j=5/2$ manifold within separate 2+ and 3+ energy windows. The analysis is outlined in Fig. 8 for the case of $YbCu_2Si_2$. A Shirley background (dashed line) is first subtracted from the raw spectrum (solid symbols). The difference spectrum (empty symbols) is then decomposed into Yb^{2+} and Yb^{3+} components. For the former, we used a Voigt line shape with an energy width [full width at half-maximum (FWHM)] $\Delta E=1.45$ eV. The line shape of the complex Yb^{3+} multiplet was phenomenologically reproduced by the sum of four Voigt functions. Finally, we used a Gaussian line shape of width $\Delta E=15$ eV (FWHM) to describe the broad plasmon feature. The quality of the fits, illustrated by the example of Fig. 8, was quite satisfactory.

When the experimental results from the various spectroscopies, summarized in Fig. 4, are compared, the RIXS

TABLE I. Estimated Yb valence from high-energy spectroscopies.

	$YbAl_3$	$YbInCu_4$	$YbCu_2Si_2$
PES ($h\nu \leqslant 120$ eV)	2.63[a]	2.57(20 K)–2.86(300 K)[b]	2.63[a]
PES ($h\nu \geqslant 500$ eV)	2.77 (10 K)[c]; 2.65 (20 K)[d]	2.67(20 K)–2.83(300 K)[e,b]	
		2.60(20 K)–2.72(70 K)[f]	
Core-level HAXPES	2.71(180 K)[d]	2.74(10 K)–2.90(220 K)[g]	
XAS	2.78(20 K)–2.83(300 K)[h]	2.83(20 K)–2.96(300 K)[i]	2.82(20 K)–2.89(300 K)[h]

[a]Reference 12.
[b]Reference 21.
[c]Reference 14.
[d]Reference 20.
[e]Reference 19.
[f]Reference 33.
[g]Reference 22.
[h]Reference 8.
[i]Reference 34.

valence is always largest, and consistent with previous XAS data (Table I). The agreement with thermodynamic and magnetic measurements is rather good even if the 300 K value for $YbCu_2Si_2$ is still lower than the high-temperature limit expected for a T_K=40 K material, as already pointed out in Ref. 8, where the possible influence of a crystal-field effect was evoked. Our estimates agree with that reference. The observation of temperature-driven valence changes in two materials with rather different characteristic energy scales like $YbAl_3$ and $YbCu_2Si_2$ is actually consistent with a Kondo scenario. For $YbAl_3$, the experiment explored a temperature range from $T > T_K$ to $T \ll T_K$, while for $YbCu_2Si_2$ the temperature varied from $T \gg T_K$ to $T \sim T_K$. In both cases, one expects to observe a sizeable part of the total temperature dependence.[4] As to photoemission, there is a considerable scattering in the literature (Table I), with low-energy PES results generally showing lower valences than soft- and hard-x-ray PES. Our core-level results are consistent with the latter, and smaller by 0.05 to 0.1 than the RIXS values. We can compare our findings with the results of a previous 3*d* core-level HAXPES study, performed on scraped surfaces of Ce IVC's.[31] There, it was found that the spectra evolved toward an almost bulk-sensitive mode when the photon energy was increased from 1 to 3.8 keV. At the higher energy, the estimated correction on the calculated valence due to the finite probing depth was 17%. The discrepancy found here with respect to the bulk-sensitive probes is similar, or even slightly larger. The increased bulk sensitivity at the larger photon energy is apparently more than compensated by a broader perturbed region in Yb materials. The HAXPES data points of Fig. 4 are too sparse to confirm the sharp jump in $YbInCu_4$, suggested elsewhere.[21,22] At present, the low signal forbids a continuous *T*-dependent HAXPES measurement.

The VB spectra yield consistently lower values than the 3*d* core data, suggesting that the 4*f* spectrum is especially sensitive to surface disorder, as also implied by many low-energy PES data. In $YbAl_3$, this difference may also point to an inadequate background removal procedure. This problem is especially delicate in HAXPES. For instance, the ratio of the Yb(4*f*) and Al(3*s*) atomic cross section decreases by one order of magnitude between 1000 and 6000 eV.[32] A comparison with Lu or La sister compounds would therefore be desirable. The difference is smaller for $YbCu_2Si_2$ and $YbInCu_4$. In the latter, the valence transition is smeared over 50 K, which again suggests the possible shortcomings of scraping the surface, even at the large photon energies and with the increased probing depth of HAXPES. Remarkably, the measured relative valence changes are quite similar for all techniques. This suggests further systematic studies on cleaved samples and at still higher photon energies. From the thoretical side, first-principles calculations of the PES and XAS spectra, including dynamical effects,[35] would reduce the uncertainties of the present analysis. They could reveal possible systematic differences between the two spectroscopic probes, namely the influence of the different final states on the estimated valence. More generally, reliable calculations of the PES and XAS/RIXS spectral functions for lattice models are also needed to clarify the discrepancies with the AIM pointed out, e.g., in Refs. 12 and 20, and to quantify the importance of coherence effects.

IV. CONCLUSIONS

We have presented a comparison of photon-in–photon-out and high-energy PES results in three representative IVC's. The data generally display a temperature and T_K dependence consistent with a Kondo scenario, and quite similar values for the relative valence changes. They also show quantitative differences. HAXPES is much more bulk-sensitive than standard PES, and provides a unique and direct view of the 4*f* many-body spectral features. However we find that, even at photon energies as high as ~6 keV, the results are probably influenced by near-surface disorder. The hope of relaxing the severe constraints imposed on photoemission by the need for cleaved single-crystal surfaces is not yet fulfilled, at least for the very testing case of Yb Kondo systems. On the other hand, RIXS and high-resolution PFY-XAS yields 4*f* occupancies that are quite consistent with thermodynamic results, and therefore appear as very attractive probes of the electronic structure of intermediate valence materials.

ACKNOWLEDGMENTS

We gratefully acknowledge the expert support of the ESRF staff. This work has been supported by the Swiss National Science Foundation and by the NCCR MaNEP. LANL support was provided by the U.S. DOE under OBES.

[1] A. C. Hewson, *The Kondo Problem to Heavy Fermions* (Cambridge University Press, Cambridge, 1993).
[2] J. W. Allen, S. J. Oh, O. Gunnarsson, K. Schönhammer, M. B. Maple, M. S. Torikachvili, and I. Lindau, Adv. Phys. **35**, 275 (1986).
[3] D. Malterre, M. Grioni, and Y. Baer, Adv. Phys. **45**, 299 (1996).
[4] N. E. Bickers, D. L. Cox, and J. W. Wilkins, Phys. Rev. B **36**, 2036 (1987).
[5] A. N. Tahvildar-Zadeh, M. Jarrell, and J. K. Freericks, Phys. Rev. Lett. **80**, 5168 (1998).
[6] J. Röhler, J. Magn. Magn. Mater. **47-48**, 175 (1985).
[7] E. Beaurepaire, J. P. Kappler, and G. Krill, Solid State Commun. **57**, 145 (1986).
[8] J. M. Lawrence, G. H. Kwei, P. C. Canfield, J. G. DeWitt, and A. C. Lawson, Phys. Rev. B **49**, 1627 (1994).
[9] J. C. Fuggle, F. U. Hillebrecht, Z. Zolnierek, R. Lässer, Ch. Freiburg, O. Gunnarsson, and K. Schönhammer, Phys. Rev. B **27**, 7330 (1983).
[10] C. Dallera, M. Grioni, A. Shukla, G. Vankó, J. L. Sarrao, J. P. Rueff, and D. L. Cox, Phys. Rev. Lett. **88**, 196403 (2002).
[11] O. Gunnarsson and K. Schönhammer, Phys. Rev. B **28**, 4315 (1983).
[12] J. J. Joyce, A. B. Andrews, A. J. Arko, R. J. Bartlett, R. I. R. Blythe, C. G. Olson, P. J. Benning, P. C. Canfield, and D. M. Poirier, Phys. Rev. B **54**, 17515 (1996).
[13] J. J. Joyce, A. J. Arko, L. A. Morales, J. L. Sarrao, and H. Höchst, Phys. Rev. B **63**, 197101 (2001); F. Reinert, R. Claessen, G. Nicolay, D. Ehm, S. Hüfner, W. P. Ellis, G.-H. Gweon, J. W. Allen, B. Kindler, and W. Assmus, *ibid.* **58**, 12808 (1998); **63**, 197102 (2001).
[14] L. H. Tjeng, S.-J. Oh, E.-J. Cho, H.-J. Lin, C. T. Chen, G.-H. Gweon, J.-H. Park, J. W. Allen, T. Suzuki, M. S. Makivić, and D. L. Cox, Phys. Rev. Lett. **71**, 1419 (1993).
[15] P. Weibel, M. Grioni, D. Malterre, B. Dardel, Y. Baer, and M. J. Besnus, Z. Phys. B: Condens. Matter **91**, 337 (1993).
[16] S.-J. Oh, Physica B **186-188**, 26 (1993).
[17] E. Weschke, C. Laubschat, T. Simmons, M. Domke, O. Strebel, and G. Kaindl, Phys. Rev. B **44**, 8304 (1991).
[18] A. Sekiyama, T. Iwasaki, K. Matsuda, Y. Saitoh, Y. Onuki, and S. Suga, Nature (London) **403**, 396 (2000).
[19] H. Sato, K. Yoshikawa, K. Hiraoka, M. Arita, K. Fujimoto, K. Kojima, T. Muro, Y. Saitoh, A. Sekiyama, S. Suga, and M. Taniguchi, Phys. Rev. B **69**, 165101 (2004).
[20] S. Suga, A. Sekiyama, S. Imada, A. Shigemoto, A. Yamasaki, M. Tsunekawa, C. Dallera, L. Braicovich, T.-L. Lee, O. Sakai, T. Ebihara, and Y. Onuki, J. Phys. Soc. Jpn. **74**, 2880 (2005).
[21] S. Schmidt, S. Hüfner, F. Reinert, and W. Assmus, Phys. Rev. B **71**, 195110 (2005).
[22] H. Sato *et al.*, Phys. Rev. Lett. **93**, 246404 (2004).
[23] A. Kotani and S. Shin, Rev. Mod. Phys. **73**, 203 (2001).
[24] I. Felner and I. Nowik, Phys. Rev. B **33**, 617 (1986).
[25] J. L. Sarrao, C. D. Immer, C. L. Benton, Z. Fisk, J. M. Lawrence, D. Mandrus, and J. D. Thompson, Phys. Rev. B **54**, 12207 (1996).
[26] P. Torelli, M. Sacchi, G. Cautero, M. Cautero, B. Krastanov, P. Lacovig, P. Pittana, R. Sergo, R. Tommasini, A. Fondacaro, F. Offi, G. Paolicelli, G. Stefani, M. Grioni, R. Verbeni, G. Monaco, and G. Panaccione, Rev. Sci. Instrum. **76**, 023909 (2005).
[27] K. Hämäläinen, S. Manninen, S. P. Collins, and M. J. Cooper, J. Phys.: Condens. Matter **2**, 5619 (1990).
[28] K. Hämäläinen, D. P. Siddons, J. B. Hastings, and L. E. Berman, Phys. Rev. Lett. **67**, 2850 (1991).
[29] C. Dallera, E. Annese, J.-P. Rueff, A. Palenzona, G. Vankó, L. Braicovich, A. Shukla, and M. Grioni, Phys. Rev. B **68**, 245114 (2003).
[30] M. Sacchi, F. Offi, P. Torelli, A. Fondacaro, C. Spezzani, M. Cautero, G. Cautero, S. Huotari, M. Grioni, R. Delaunay, M. Fabrizioli, G. Vankó, G. Monaco, G. Paolicelli, G. Stefani, and G. Panaccione, Phys. Rev. B **71**, 155117 (2005).
[31] L. Braicovich, N. B. Brookes, C. Dallera, M. Salvietti, and G. L. Olcese, Phys. Rev. B **56**, 15047 (1997).
[32] J. J. Yeh and I. Lindau, At. Data Nucl. Data Tables **32**, 1 (1985).
[33] D. P. Moore, J. J. Joyce, A. J. Arko, J. L. Sarrao, L. Morales, H. Höchst, and Y. D. Chuang, Phys. Rev. B **62**, 16492 (2000).
[34] A. L. Cornelius, J. M. Lawrence, J. L. Sarrao, Z. Fisk, M. F. Hundley, G. H. Kwei, J. D. Thompson, C. H. Booth, and F. Bridges, Phys. Rev. B **56**, 7993 (1997).
[35] O. Wessely, M. I. Katsnelson, and O. Eriksson, Phys. Rev. Lett. **94**, 167401 (2005).